

ORIGINAL RESEARCH ARTICLE

Fortified trabeculae-like biomimetic bone-filling material organoids for repair of weight-bearing bone defects

Chong Yin^{1,2}, Xingyu Wang², Jing Zhang², Yang Yu³, Linfeng Liu², Hongqi Han², Guilin Luo², Zhuo Guo², Yingying Luo², Conghui Jiang², Ye Tian⁴, Rui Pang², Jingxiang Li², Wei Chen^{5*}, Bing Yang^{6*}, Xundong Deng^{4*}, Bing Guo^{1,2*}, and Guangrong Wang^{1,2*}

¹Department of Clinical Laboratory, Department of Oncology, Affiliated Hospital of North Sichuan Medical College, Nanchong, Sichuan, China

²Department of Laboratory Medicine, Translational Medicine Research Center, North Sichuan Medical College, Nanchong, Sichuan, China

³Department of Medical and Nursing Science, International School, Krirk University, Bangkok, Thailand

⁴Lab for Bone Metabolism, Xi'an Key Laboratory of Special Medicine and Health Engineering, Key Lab for Space Biosciences and Biotechnology, Research Center for Special Medicine and Health Systems Engineering, NPU-UAB Joint Laboratory for Bone Metabolism, School of Life Sciences, Northwestern Polytechnical University, Xi'an, Shaanxi, China

⁵Xinjiang Hua Shidan Drug Research Co., Urumqi, Xinjiang, China

⁶Department of Public Health, International School, Krirk University, Bangkok, Thailand

*Corresponding authors: Guangrong Wang (13699669835@163.com); Bing Yang (yang.bing@krirk.ac.th); Wei Chen (www.chen-001@163.com); Bing Guo (guobin@nsmc.edu.cn); Xundong Deng (dengxd@nwpu.edu.cn)

Citation: Yin C, Wang X, Zhang J, *et al.* Fortified trabeculae-like biomimetic bone-filling material organoids for repair of weight-bearing bone defects. *Organoid Res.* 2026;2(2):026110016. doi: 10.36922/OR026110016

Received: March 11, 2026

Revised: June 5, 2026

Accepted: June 11, 2026

Published online: June 30, 2026

Copyright: © 2026 Author(s). This is an Open-Access article distributed under the terms of the Creative Commons Attribution License, permitting distribution, and reproduction in any medium, which provided that the original work is properly cited.

Publisher's Note: AccScience Publishing remains neutral with regard to jurisdictional claims in published maps and institutional affiliations.

Abstract

Repairing critical-sized bone defects remains challenging, and many synthetic fillers trade mechanical stability against bioactivity. In this study, a novel bone tissue-filling material was designed and synthesized. Based on a previously described trabeculae-like biomimetic bone-filling material (TBM), mammoth tusk dentin was incorporated into this material, which endowed it with enhanced mechanical properties. We designated this material as fortified TBM (FTBM). FTBM demonstrated favorable mechanical strength, biocompatibility, and sustained drug-release capacity, thereby improving osteogenesis. In addition, human mesenchymal stem cells were encapsulated within the scaffold, resulting in a cell-laden biomaterial. Its efficacy in repairing bone defects was superior to the original TBM. This high-hardness bone-filling material offers a strategy to enhance the mechanical stability of trabeculae-like fillers, warranting evaluation in load-bearing models.

Keywords: Bone-filling material; Mammoth tusk dentin; Osteogenesis; Bone defect

1. Introduction

As the primary supporting structure of the human body, bone plays key roles in maintaining locomotor function, hematopoiesis, and various other physiological processes.¹ Bone defects can arise from trauma, infection, tumor, and other bone disorders. Critical-sized bone defects

usually cannot heal spontaneously via intrinsic self-repair mechanisms.^{2,3} Consequently, due to difficulties with treatment and slow recovery, bone defects impose heavy burdens on individuals and families. Therefore, treating such bone defects more accurately and efficiently is challenging for clinicians.

In situ repair with bone-filling materials is an effective strategy for treating bone defects. These materials fill defect areas, provide mechanical support and promote bone formation.^{4,5} Although autologous or allogeneic bone transplantation has long been the optimal choice for bone defect repair⁶, its widespread use is limited by insufficient donor sources and the risks of secondary injury and infection.⁷ Consequently, synthetic bone-filling materials have been developed, such as the gelatin methacryloyl–hydroxyapatite/beta-tricalcium phosphate composite that is widely used clinically.⁸ Although existing bone-filling materials satisfy most clinical demands, materials with higher hardness and enhanced osteogenesis properties are required under certain conditions, including emergency load-bearing after cervical and lumbar surgery.^{9,10} Thanks to advances in bone tissue engineering and organoid technology, novel composite bone-filling materials have been developed.^{11,12} These materials are centered on biomimetic, multifunctional and intelligent design^{13,14}, including nano-composite strengthening (e.g., hydroxyapatite–boron nitride nanotube–carboxymethyl cellulose)¹⁵, biomimetic ion doping (Mg, Si, Sr, etc.)¹⁶, bioglass/metal–matrix composites^{17,18}, polymer–matrix nanocomposites.^{19,20} Thus, these systems face inherent challenges in terms of balancing hardness and osteogenesis.

To address such limitations, we designed and prepared a novel bone tissue-filling material, or fortified trabeculae-like biomimetic bone-filling material (FTBM). This material was fabricated by incorporating mammoth tusk dentin into the porous scaffold structures of our previously developed TBM.² Mammoths are extinct prehistoric proboscideans with ivory tusks of 3–5 m long. Their tusk dentin is dense and very hard. Mammoth remains are primarily found in high-latitude regions of the Northern Hemisphere (e.g., Siberia). Currently, mammoth ivory is derived from permafrost-preserved remains and is mainly used for ivory carving, jewelry making, and scientific research.^{21,22} The material used here came from processing jewelry and other product leftovers, and at approximately 50–80 USD/kg, it was inexpensive and had a relatively stable supply. In contrast to African ivory, which has irregular sources, is expensive, yields little, and is non-renewable, mammoth ivory trade/use is legal and compliant, and, importantly, its acquisition does not harm living animals.

In this study, by adding mammoth tusk dentin to porous scaffold structures in our previously developed TBM², we fabricated FTBM, a novel bone tissue-filling material with significantly improved mechanical properties. FTBM retained porous structures highly similar to natural bone trabeculae in both structure and function, and possessed high biocompatibility, mechanical strength, and drug-loading capacity. FTBM served as a carrier for human mesenchymal stem cells (hMSCs) and promoted

osteogenesis in mouse calvarial and tibial defect models. Our study highlights the development of bone-filling materials.

2. Materials and methods

2.1. Reagents

All reagents and cells used in this study are listed as follows: hMSCs (Runde Biotechnology Co., Ltd., China), nucleic acid delivery system (polyvinylamine [PVAm], gift from Prof. D. Xudong, Northwestern Polytechnical University), novel recombinant antagomiR-138-5p (nCAR-anti-138 [anti138]; RQCON Biological Technology Co., Ltd, China), Cell Counting Kit-8 (CCK-8; Beyotime Biotechnology Co., Ltd., China), 4% paraformaldehyde and collagenase II (BioSharps, China), dimethyl sulfoxide (DMSO) and glycerol (BioFroxx, China), fetal bovine serum (FBS), trypsin and Dulbecco's Modified Eagle's Medium (DMEM; Gibco, United States), biphasic calcium phosphate (BCP, DULY, China), fluorescein amidite-labeled small interfering RNA-negative control (FAM-labeled siRNA-NC; GenePharma, China), as well as bergamottin (Ber; B757586, Aladdin, China), chitosan (C8320, Solarbio, China) and rhodamine B (R104960, Aladdin, China).

2.2. Fortified trabeculae-like biomimetic bone-filling material preparation

Mammoth ivory (Unified Social Credit Code: 92150928MA0QXG9CXB, Zhongyi Mengma Art and Antique Shop, China) fragments were cut into irregular pieces (0.25–0.5 cm³) using a bone saw. After grinding in a mortar, the pieces were further ground in liquid nitrogen, then re-ground in a mortar to obtain powder, which was sieved through 100- and 400-mesh screens to obtain 100- or 400-mesh powders. The powder was sterilized with ultraviolet light overnight. Next, a 7% silk protein solution, a 2% chitosan solution, and Matrigel (Corning, United States) were mixed and immediately supplemented with an equal weight (1:1) mixture of BCP and mammoth ivory powder (in contrast, TBM was composed of BCP alone at the same weight). After thorough stirring at 65 °C, the mixture was frozen at –80 °C, soaked in water, and re-lyophilized (without a freezing step) to generate a core-pillar structure (Core). This was used as a scaffold and covered with the same mixture (plus 0.1% methacrylated RGD peptide) on peripheral surfaces. After stirring (at 65 °C), freezing, lyophilizing, and soaking, the material was re-lyophilized after freezing (–80 °C for 30 min) to generate a trabeculae-like porous skeletal structure. Hyaluronic acid methacrylate (HAMA) hydrogel containing 0.1% methacrylated RGD peptide carrying water-soluble agents or DMSO-dissolved lipophilic drugs with photoinitiator Irgacure 2959 (I2959) was coated on porous skeletons and cross-linked via ultraviolet light to produce FTBM.

2.3. Fortified trabeculae-like biomimetic bone-filling characterization

For scanning electron microscopy (SEM), FTBM micromorphology was examined at 3 kV using a Gemini300 SEM (Zeiss, Germany). Elemental composition was processed using energy-dispersive X-ray spectroscopy (EMX; Horiba, France). Swelling ratios were calculated using Equation 1²³:

$$(W_N - W_0)/W_0 \times 100\% \quad (1)$$

where W_0 is the initial material weight, and W_N is the water-soaked material weight.

Degradation ratios were calculated using Equation 2²³:

$$(W_0 - W_N)/W_0 \times 100\% \quad (2)$$

where W_0 is the initial material weight, and W_N is the collagenase II-treated material weight.

2.4. Mechanical characterization of fortified trabeculae-like biomimetic bone-filling material

Atomic force microscopy and room-temperature compression were used to investigate the mechanical characterization of FTBM. For atomic force microscopy, 400-mesh mammoth ivory powder was fixed to the substrate (Dimension Icon, Bruker, United States). A probe was used to scan and record the modulus information on the sample surface.

For room-temperature compression, the prepared TBM or FTBM was fixed in the universal testing machine (Shimadzu AGX, Shimadzu, Japan) and compressed at a loading rate of 5 mm/min to record the stress-strain curve until failure.

2.5. Slow-release measurements

Fortified trabeculae-like biomimetic bone-filling material scaffolds loaded with fluorescent labels, including 5 µg/mL rhodamine B or 100 µM FAM-NC, were rinsed with deionized water over 0.5 h, then immersed in 1,000 µL ultrapure water; the incubation temperature was set at 4 °C except that the rhodamine B release experiment was performed under ambient temperature to complete sustained release detection. Slow-release medium was collected periodically, and the FTBM was re-added to 1,000 µL deionized water to facilitate slow-release processes. Sample fluorescence was measured using the SpectraMax Paradigm microplate reader (Molecular Devices, United States).

2.6. Polyvinylamine preparation

A PVAm (Xelorex RS 1100, ~57 kDa, Solenis Sweden AB,

Sweden) aqueous solution (molecular weight = 1,100 and concentration = 10%) was dialyzed (molecular weight cutoff < 10,000), passed through a syringe (5 µm), lyophilized to a purified PVAm powder before being diluted with distilled water to 0.9 mg/mL.²⁴

2.7. Cell culture

Human MSCs were maintained in high-glucose DMEM (KeyGEN BioTECH, China) supplemented with 10% FBS (OPCEL, China) and 1% penicillin/1% streptomycin (Amresco, United States) at 100% density, and osteogenically induced in osteogenic medium plus DMEM, 10% FBS, 1% penicillin/1% streptomycin, 1% L-glutamine, 1% ascorbic acid (Sigma, United States), and 1% β-glycerophosphate (Sigma, United States).

2.8. Cell Counting Kit-8 and flow cytometry assay

Fortified trabeculae-like biomimetic bone-filling material-related cell viability was examined using CCK-8 assays. hMSCs were treated with HAMA or FTBM in 96-well plates, after which cells were incubated with DMEM plus CCK-8 solution (10%) for four h. Subsequently, the medium (100 µL) was removed, and absorbance was measured at 450 nm using a Sunrise™ microplate reader (TECAN, Switzerland).

For flow cytometry, hMSCs were grown for 48 h with FTBM, digested (trypsin), fixed in 70% ethanol (ice-cold), washed, and stained in propidium iodide (PI; 0.1 mg/mL). Cell cycle processes were then examined using a FACS Calibur Flow Cytometer (BD Biosciences, United States).²⁵

2.9. Hemolysis assays

Anti-coagulated blood was collected from C57BL/6 mice (Huafukang Bioscience Co., Ltd., China) and centrifuged, from which pure erythrocytes were suspended in phosphate-buffered saline (PBS), and FTBM was added. All suspension samples were kept at 37 °C for a three-h incubation period, after which supernatants were photographed and absorbances were recorded.²⁶

2.10. Embedding of cells in fortified trabeculae-like biomimetic bone-filling material

Hyaluronic acid methacrylate in cell suspension was crosslinked and overlaid on a porous frame to generate hMSC-embedded FTBM. This hMSC-embedded FTBM was then added to a microfluidic system or subcutaneously implanted onto the calvarial surfaces of mice (mice received hMSC-embedded FTBM). CCK-8 assays were then conducted to assess cell viability. For cell extraction from FTBM, FTBM fragments were shredded and submerged in complete culture medium to separate cells, which then grew and adhered to surfaces.

2.11. Fortified trabeculae-like biomimetic bone-filling material cell viability assays

To qualitatively assess FTBM-associated cell viability, a calcein AM/PI Live/Dead cell staining test kit (KeyGEN BioTECH, China) was used. After rinsing with PBS, FTBM samples were incubated in the dark for 30 min at ambient temperature with 2×10^{-6} M calcein AM and 4×10^{-6} M PI working solution. Sections (4- μ m thick) were observed using confocal microscopy (FV3000, Olympus, Japan).

2.12. 5-Ethynyl-2'-deoxyuridine labelling assays for fortified trabeculae-like biomimetic bone-filling material

To examine cell proliferation, a 5-Ethynyl-2'-deoxyuridine (EdU) labelling/detection kit (RiboBio, China) was used. FTBM-embedded hMSCs were grown in 24-well plates; then 50 μ M EdU was added, and cells were incubated for 12 h at 37 °C. Next, the FTBM-embedded cells were fixed in 4% formaldehyde for 30 min at 37 °C and treated with 0.5% Triton X-100 (Sigma-Aldrich, United States) for 30 min at 37 °C. After PBS washes ($\times 3$), 100 μ L of a 1 \times Apollo reaction cocktail was added, and cells were incubated for 45 min at 37 °C. Subsequently, cells were stained with 100 μ L of Hoechst 33342 (C10310, RiboBio, China) for 30 min at 37 °C. Cells were visualized using confocal microscopy (FV3000, Olympus, Japan). Cells were gamma-adjusted, merged with Hoechst staining, and analyzed in Image-Pro Plus 6.0 software (United States). The ratio of EdU-positive cells to total Hoechst-positive cells indicated EdU incorporation. Experiments (triplicate) were performed three times.

2.13. Immunofluorescence

As previously described, FTBM (2 mm³ pieces) underwent immunofluorescence in 96-well plates²⁷ using alkaline phosphatase (ALP; ET1601-21, HUABIO, China), Runt-related transcription factor 2 (RUNX2; ET1612-47, HUABIO, China), actin (BL005B, Biosharp, China), and a fluorescently labelled secondary antibody (20000259, CoraLite 488-conjugated goat anti-rabbit; 1:100; Proteintech, United States). Cells were observed by laser-scanning confocal microscopy (FV3000, Olympus, Japan) at 488 nm and 405 nm.

2.14. Immunohistochemistry

CD3 (1:100; sc-20047, RRID: AB_627014) and CD68 mouse (1:100; sc-20060, RRID: AB_627158) monoclonal antibodies (Santa Cruz Biotech, United States) were used. Primary antibody incubation was performed overnight at 4 °C, whereas secondary antibody incubation was performed for 1.5 h at room temperature.

2.15. Reverse transcription polymerase chain reaction

Reverse transcription polymerase chain reaction (RT-PCR) was used to examine osteogenic differentiation in hMSCs. Total RNA was extracted using E.Z.N.A.[®] Total RNA Kit I (Omega Bio-TEK, United States) and transcribed to complementary DNA using HiScript[®] II 1st Strand cDNA Synthesis Kit (Vazyme, China), after which RT-PCR was conducted using ChamQ Universal SYBR qPCR Master Mix (Vazyme, China). Tsingke, Inc. (China) provided the primers (Table S1).

2.16. Western blotting

After FTBM-embedded hMSCs were lysed, the lysates were resolved by electrophoresis, and proteins were transferred to nitrocellulose membranes. Protein-bearing membranes were blocked with 5% skim milk solution, incubated at 4 °C overnight with primary antibody solutions, and then incubated with horseradish peroxidase-conjugated secondary antibodies. Protein bands, identified using enhanced chemiluminescence (Biosharp, China), were exposed on a Fusion FX imager (Vilber Lourmat, France). Antibodies (HUABIO) were used at 1:2,000 dilutions: ALP (ET1601-21, HUABIO, China), RUNX2 (ET1612-47, HUABIO, China), and GAPDH (T1601-4, RRID: AB_3069615, HUABIO, China). Horseradish peroxidase-conjugated anti-immunoglobulin G antibodies (1:2,000; CW0102-RRID-AB_2814710 and CW0103-RRID-AB_2814709, CWBIO, China) were also used.

2.17. Alkaline phosphatase staining

After 48 h of culture, cells were harvested, fixed in 10% buffered formaldehyde for 20 min, washed (3 \times) in PBS (pH 7.4) for five min each, and stained with 5-bromo-4-chloro-3-indolyl phosphate/nitro blue tetrazolium solution. Reactions were terminated in distilled water, after which cells were imaged on a scanner to detect intracellular ALP levels.²²

2.18. Alizarin Red S staining

When the hMSCs co-cultured with FTBM were in logarithmic phase, they were seeded into plates. After 12 h, various materials were added to the continuous culture. For osteogenic differentiation, hMSCs were cultured in mineralized medium (10% FBS, 1% penicillin/streptomycin, 50 μ g/mL ascorbic acid, and 10 mM β -glycerophosphate) for approximately 14–21 days. The cells were then fixed in 4% paraformaldehyde, washed in PBS (3 \times), stained in 0.5% alizarin solution (pH 4.2) for 15–30 min, washed in deionized water (3 \times), air-dried, and scanned.²²

Alizarin Red-Alcian Blue staining and Safranin O staining were adopted to detect hMSC distribution in FTBM. For Alizarin Red-Alcian Blue Staining, FTBM

fragments were first stained with Alcian Blue (Beyotime, China) at pH 2.5. After washing, fragments were incubated with Alizarin Red S (Beyotime, China) in a 2% solution at pH 4.2, followed by thorough rinsing with distilled water to remove excess dye. The fragments were then transferred to a glass slide and viewed under optical microscopy (Nikon 80i, Tokyo, Japan).

Safranin O Staining was performed using the staining kit (Beyotime, China) according to the manufacturer's instructions. In brief, fragments were first stained with Fast Green, then briefly rinsed with acetic acid. Subsequently, Safranin O was applied; the fragments were treated with acetic acid solution, transferred to a glass slide, and viewed under optical microscopy (Nikon 80i, Tokyo, Japan).

2.19. Therapeutic fortified trabeculae-like biomimetic bone-filling material in mice

We used 120 two-month-old male C57BL/6 mice (25 ± 0.5 g, Huafukang Bioscience Co., Ltd., China). For the bone defect model, a dental drill was used to create standardized 1.2 mm defects in mouse tibiae or calvariae.²⁸ FTBM was then directly implanted into bone defect regions without cells. For blank group, bone defect mice were untreated, for FTBM group mice were implanted with normal FTBM, for Ber group, mice were implanted with FTBM append with 200nM bergamottin, for PVAm group, mice were implanted with FTBM append with 0.09 mg/ml polyvinylamine, for MSA group, mice were implanted with FTBM append with 0.09 mg/ml polyvinylamine and 100 μ M empty recombinant tRNA (MSA), for anti138 group, mice were implanted with FTBM append with 0.09 mg/ml polyvinylamine and 100 μ M nCAR-anti-138. After 12 days (when comparing TBM to FTBM: four weeks), mice were humanely euthanized (in carbon dioxide). Animal care/procedures were sanctioned by the North Sichuan Medical College Ethics Committee (No. 2023078). At all times, we minimized the number of mice and their suffering during animal studies.

2.20. Hydrogel biocompatibility *in vivo*

For blood chemical analyses, mouse blood supernatants were measured for aspartate aminotransferase (AST), alanine aminotransferase (ALT), blood urea nitrogen (BUN), and creatinine (Cr) (ADVIA 2400 Chemistry System, Siemens Healthcare Diagnostics, United States). Heart, liver, spleen, lung, and kidney samples were also fixed and paraffin-embedded for hematoxylin & eosin (H&E) staining and viewed under optical microscopy (Nikon 80i, Tokyo, Japan).

2.21. Bone histomorphometric analyses

Fortified trabeculae-like biomimetic bone-filling material-mediated effects on bone repair were examined using

double calcein labelling²⁹ and micro-computed tomography (v.6.5, Viva CT40, Scanco Medical, Switzerland), the latter of which was used to assess bone microstructures and bone defect regions. Images were reconstructed/calibrated at an isotropic voxel size = 10.5 μ m (70 kVp, 200 ms integration time, 1,200 mg HA/cm³, 260 thresholds, and 114 μ A). Using Scanco evaluation software, defined bone defect regions were manually examined by contouring three-dimensional reconstructions (sigma = 1.2, supports = 2, and threshold = 200) to estimate bone volume to tissue volume (BV/TV), bone mineral density (BMD), and bone mineral content (BMC).³⁰

2.22. Statistical analyses

All experiments were performed on at least three independent occasions, and each experiment was performed in triplicate. Samples and experimental animals were randomly distributed to each group. Investigators were blinded to group allocation during data collection. Samples were excluded from statistical analysis in the following cases: accidental death of experimental mice, cell contamination, sample loss, and outlier data points beyond the mean \pm standard deviation (SD) range.

All quantitative data are presented as mean \pm SD, and error bars in all figures represent SD. An independent Student's *t*-test was used for comparisons between two groups. For comparisons involving three or more groups, one-way analysis of variance was applied, followed by Tukey's HSD post hoc multiple comparisons test for pairwise comparisons. Uniform significance thresholds were adopted throughout this study: **p* < 0.05, ***p* < 0.01, ****p* < 0.001. The abbreviation ns (not significant) indicates no statistically significant difference. All statistical analyses were performed using GraphPad Prism 10.1.2 software.

Only male C57BL/6 mice were used for the *in vivo* evaluation of bone repair in this study, as estrogen and other sex hormones can affect bone metabolism.

3. Results

3.1. Fortified trabeculae-like biomimetic bone-filling material construction and characterization

The material was fabricated using silk fibroin, chitosan, base gel, biphasic calcium phosphate, mammoth tusk dentin, and HAMA. Silk fibroin solution, biphasic calcium phosphate, mammoth tusk dentin powder, chitosan solution, and base gel were mixed uniformly, and a porous scaffold structure was formed via the melting-phase separation method. Finally, the porous scaffold was coated with HAMA hydrogel to obtain the mammoth ivory-based artificial bone-filling material. SEM images showed that the micro-scaffold material exhibited an overall trabeculae-like porous network structure, and mammoth tusk dentin

particles were uniformly distributed in the trabeculae-like porous scaffold in a polyhedral morphology. Moreover, compared with the 100-mesh group, 400-mesh-sieved ivory dentin exhibited a more regular particle size (Figure 1A). Energy-dispersive X-ray spectroscopy revealed that the mammoth ivory-based artificial bone contained carbon, phosphorus, sulfur, calcium, and other elements, with homogeneous distribution throughout the material (Figure 1B and 1C), suggesting that the material may better meet the mechanical requirements for bone defect repair.

Mechanical properties are crucial for bone repair. To verify the mechanical strength of FTBM, we conducted a compression test at room temperature. Incorporating mammoth ivory particles increased the peak compressive stress of the construct relative to TBM (0.13 vs. 0.07 MPa), representing an approximately 1.9-fold increase in ultimate compressive strength, although both values remain below the trabecular-bone range (Figure 1D–1G). The high modulus of mammoth tusk dentin provided nanoscale mechanical support for the material, effectively enhancing the mechanical properties of the composite system (Figure S1A and S1B). These mechanical advantages were particularly valuable for filling critical-sized bone defects.

Swelling is an important property of bone-filling materials. Therefore, the swelling ratio and degradation rate of HAMA, TBM, and FTBM were measured. The results showed that all materials exhibited stable swelling ratios and maintained dissolution equilibrium within 35 days (Figure S1C). Compared with the HAMA hydrogel group, FTBM showed faster degradation in the presence of collagenase II (100 U/mL), which was generally consistent with that of the TBM group (Figure S1D). This faster degradation of FTBM would be beneficial for long-term bone repair filling, drug delivery, and the promotion of bone regeneration in the defect area.

In addition to its structural function as a bone filler, FTBM exhibited excellent sustained-release capacity. Release kinetics showed that rhodamine B was released gradually and stably in the short term (Figure S1E), indicating effective diffusion from the scaffold matrix. The controlled release of nucleic acid-based therapeutics was evaluated using FAM-labeled siRNA-NC. Results confirmed that FTBM, similar to TBM, could incorporate and stably release nucleic acids over time. The addition of PVAm extended nucleic acid release from 7 days to ≥ 14 days, with the fluorescence signal retained at $\sim 78\%$ of the initial intensity on day 14 (Figure S1F). These results demonstrate that FTBM can serve as a sustained-release therapeutic platform for drug delivery-assisted bone defect repair.

3.2. Promotion of osteogenic differentiation *in vitro* by fortified trabeculae-like biomimetic bone-filling material

To evaluate the *in vitro* cytocompatibility of FTBM, the material was immersed in cell culture medium, and its effects on cell viability, cell cycle, and cell adhesion were assessed (Figure 2A). The CCK-8 assay showed that the viability of FTBM co-cultured hMSCs did not differ significantly from that of the untreated group within 72 h (Figure 2B). Cell cycle analysis revealed no significant differences among FTBM-treated, untreated, and HAMA-treated cells (Figure S2A). The hemolysis assay further confirmed that FTBM did not induce hemolysis (Figure S2B and S2C). Collectively, these results demonstrated that FTBM had excellent *in vitro* biocompatibility.

To evaluate the ability of FTBM as a carrier for osteogenic drugs, osteogenic differentiation-promoting small-molecule drug Ber and nucleic acid drug anti138 were selected and loaded.^{31–32} The osteogenic differentiation level of hMSCs after treatment with the drug-loaded material was evaluated. ALP and Alizarin Red S (ARS) staining indicated that the Ber- and anti138-loaded materials significantly elevated ALP activity and mineralized nodule formation (Figure 2C). RT-PCR analysis yielded higher expression of ALP and RUNX2 in hMSCs cultured with Ber- or anti138-loaded FTBM (Figure 2D).

To further investigate the sustained-release ability of the bone-filling material for osteogenic drugs, FTBM loaded with different drugs were immersed in complete medium for sustained release. The released medium was collected on days 7, 14, 21, and 28 and applied to hMSCs. Results showed that the material loaded with anti138 could continuously inhibit miR-138-5p levels within 28 days (Figure 2G). RT-PCR, ALP staining, and ARS staining results proved that FTBM loaded with Ber and anti138 had a long-lasting effect on promoting osteogenic differentiation. Ber-loaded FTBM maintained osteogenic promotion for 21 days, whereas the anti-138-loaded FTBM sustained the effect for 28 days (Figure 2E and 2F, 2H and 2I). These results confirmed that FTBM enabled sustained drug release and maintained long-term regulation of osteogenic differentiation.

3.3. Application of fortified trabeculae-like biomimetic bone-filling material as cell-laden scaffold

To investigate whether FTBM can serve as a cell-laden scaffold, hMSCs, which exhibit low immunogenicity, were selected as experimental cells. Cells were embedded into FTBM or HAMA and cultured in microfluidic medium (Figure 3A). After 72 h, cells embedded in the material remained highly viable (Figure 3B). EdU staining

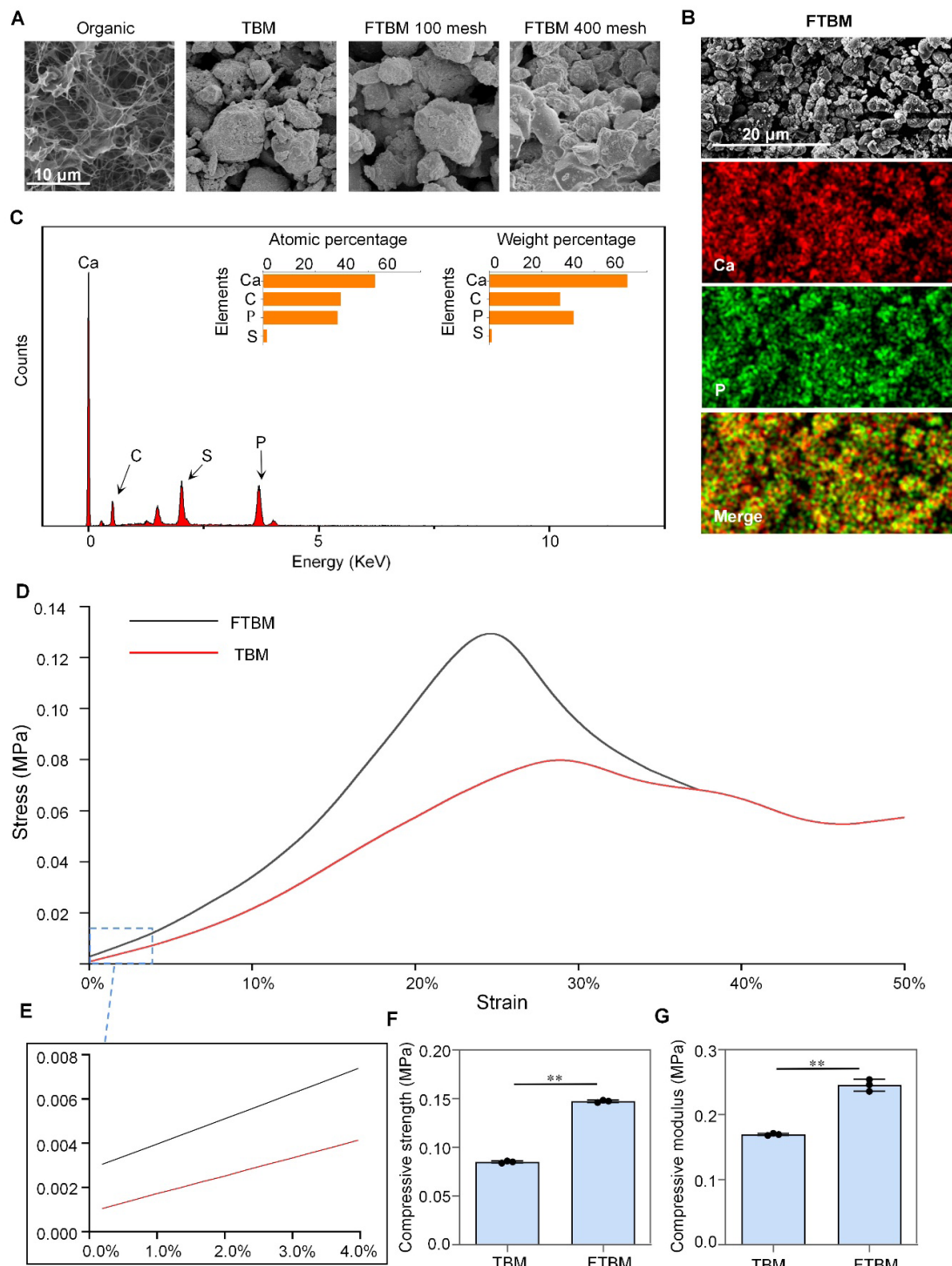


Figure 1. Characterization of fortified trabeculae-like biomimetic bone-filling material (FTBM). (A) Scanning electron microscope (SEM) images of the organic network (Organic), previously designed TBM, 100-mesh mammoth tusk dentin powder-constructed FTBM, and 400-mesh mammoth tusk dentin powder-constructed FTBM. Scale bar: 10 μm ; magnification: 1,400 \times . (B) Energy-dispersive spectroscopy mapping of FTBM. Scale bar: 20 μm ; magnification: 1,250 \times . (C) Energy-dispersive spectroscopy (EDS) spectrum of FTBM sample, with characteristic peaks of calcium, carbon, phosphorus, and sulfur labeled on the spectrum curve. The insets show bar graphs of the normalized elemental atomic percentage (Atomic %) and weight percentage (Weight %). Element quantification was normalized by setting the total content of all detected elements to 100%. (D) Stress-strain curve for cylindrical 4.5 \times 8.0 mm TBM and FTBM. (E) The zoomed-in window shows the initial slopes of the stress-strain curves in D. (F) Ultimate compressive strength as determined by the maximum load at failure. (data represented as mean \pm standard deviation; ** $p < 0.01$, $n = 3$). (G) Compressive modulus calculated using the 4% strain offset linear slope method. (data represented as mean \pm standard deviation; ** $p < 0.01$; $n = 3$).

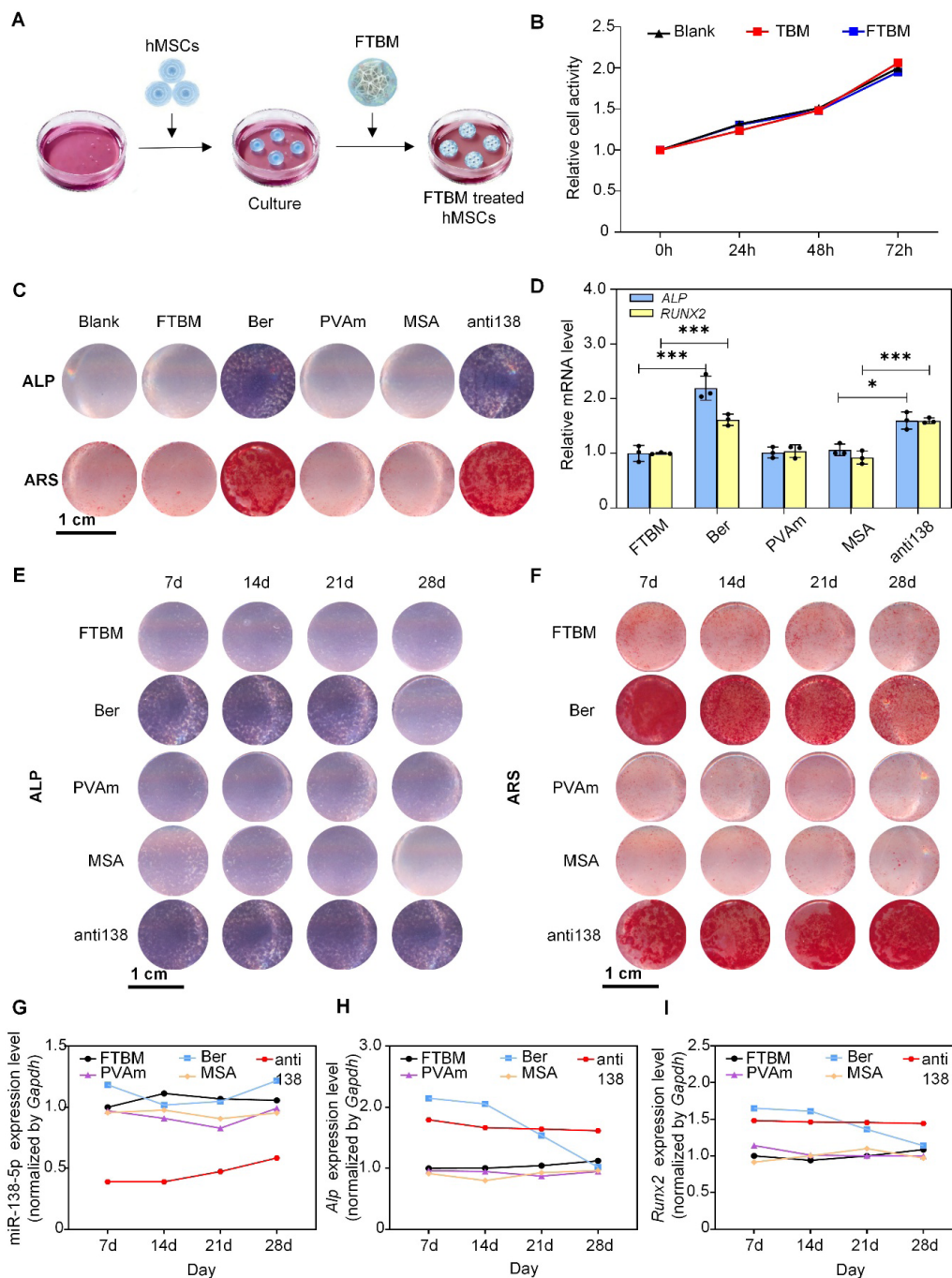


Figure 2. Drug-loaded fortified trabeculae-like biomimetic bone-filling material (FTBM) regulates osteogenic differentiation *in vitro*. (A) Schematic diagram of FTBM-induced osteogenic differentiation by loading drugs *in vitro*. (B) Viability of human mesenchymal stem cells (hMSCs) cultured with TBM or FTBM, determined by Cell Counting Kit-8 (CCK-8) assay. (C & D) Alkaline phosphatase (ALP) and Alizarin Red staining (ARS) of hMSCs treated with FTBM loaded with bergamottin (Ber) or nCAR-anti-138 (anti138). Scale bar: 1 cm; magnification: 1.28×. ALP and RUNX2 expression levels detected by (C) staining and (D) reverse transcription polymerase chain reaction (mean ± standard deviation; **p* < 0.05, ****p* < 0.001; *n* = 3). (E & F) ALP and ARS staining of hMSCs in the FTBM, Ber, polyvinylamine (PVAm), empty recombinant tRNA (MSA), and anti138 groups at different time points. Scale bar: 1 cm; magnification: 1.2×. (G–I) The expression levels of miR-138-5p (G), ALP (H), and RUNX2 (I) in hMSCs treated with slow-release solution from FTBM loaded with either Ber (compared with blank FTBM) or anti138 (compared with FTBM loaded with MSA and PVAm), detected by reverse transcription polymerase chain reaction (mean ± standard deviation; *n* = 3).

Notes: anti138: hMSCs treated with FTBM loaded with nCAR-anti-138; Ber: hMSCs treated with FTBM loaded with bergamottin; Blank: untreated hMSCs; FTBM: hMSCs treated with unmodified FTBM; MSA: Recombinant tRNA^{Met}-fused Sephadex aptamer; hMSCs treated with FTBM loaded with empty recombinant tRNA; PVAm: Polyvinylamine; hMSCs treated with FTBM loaded with PVAm.

revealed their high proliferation within seven days, while calcein-AM/PI double-staining further confirmed high cell viability over the same culture period. (Figure 3C and 3D). The distribution of hMSCs was observed via Alcian blue staining and Safranin O-fast green staining. As shown, hMSCs were observed in the hydrogel layer and on the porous scaffold structure (Figure 3E and 3F), indicating that FTBM supported the growth of hMSCs within its scaffold structure to develop into potential bone trabeculae. The cell-embedded material was further cultured *in vitro* for seven days. Actin immunofluorescence showed that

hMSCs remained viable (Figure 3G).

Human MSCs were also embedded into FTBM together with osteogenic drugs Ber or anti138. After 96 h of *in vitro* culture, intracellular ALP and RUNX2 levels were detected using immunofluorescence. Relative ALP and RUNX2 immunofluorescence signals were stronger in cells treated with drug-loaded FTBM (Figure 4A and 4B). The Ber group exhibited ALP intensity of 2.2455 and RUNX2 intensity of 2.1626, and the anti138 group showed ALP at 1.5094 and RUNX2 at 1.8260, all exceeding the reference value of 1.00 in the FTBM control. The encapsulated

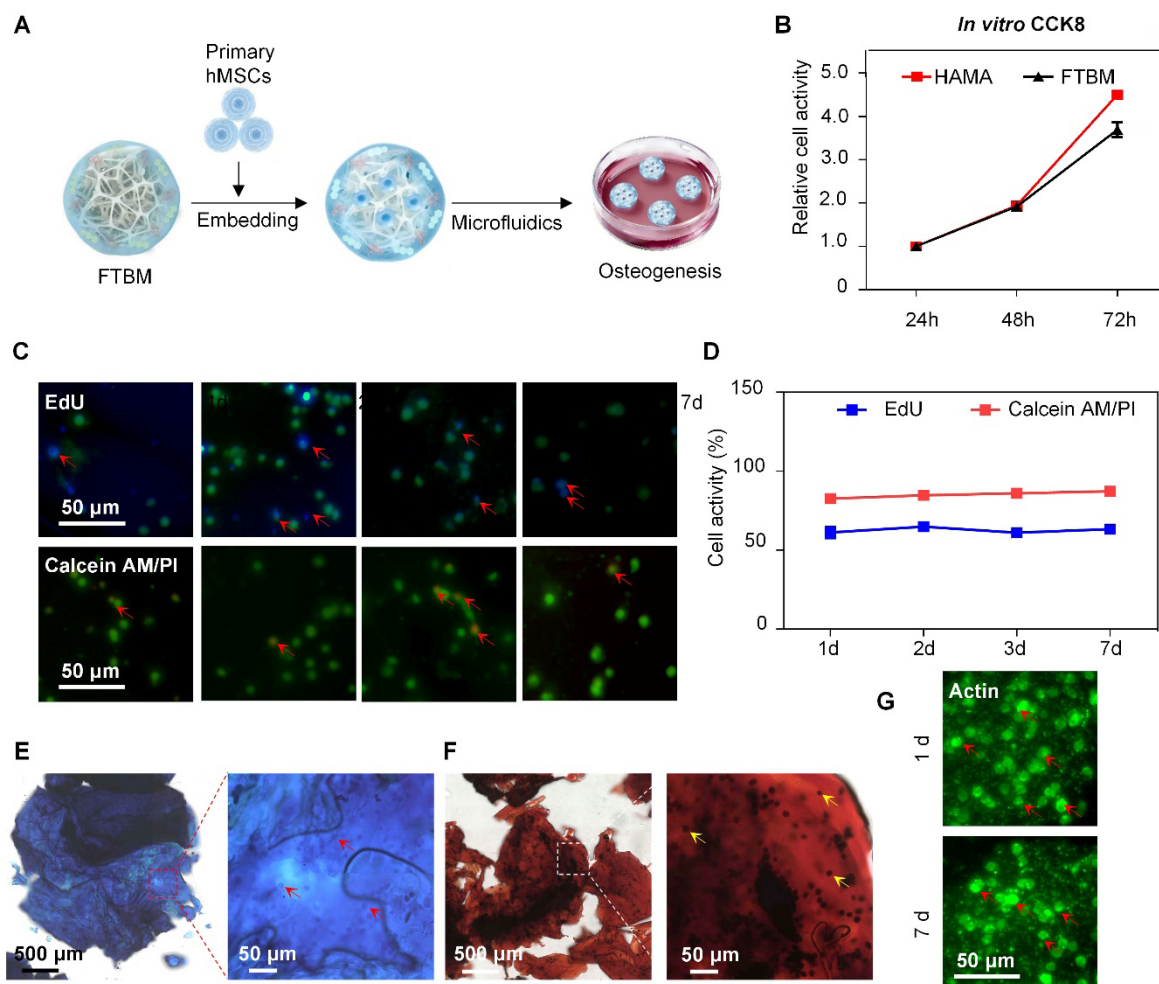


Figure 3. Fortified trabeculae-like biomimetic bone-filling material (FTBM) as a cell-laden scaffold. (A) Schematic diagram of FTBM embedding human mesenchymal stem cells (hMSCs) *in vitro*. (B) Viability of hMSCs encapsulated in hyaluronic acid methacrylate or FTBM, measured by Cell Counting Kit-8 assay. (C & D) Cell proliferation and viability of hMSCs embedded in FTBM cultured *in vitro*, as detected by 5-ethynyl-2'-deoxyuridine (EdU) staining and calcein-AM/PI staining. Scale bar: 50 μ m; magnification: 230 \times . Red arrows indicate live and dead cells in the first and second rows, respectively. (E & F) Alizarin red-Alcian blue (E) and Safranin O (F) displaying the distribution of hMSCs in the hydrogel layer and porous scaffold structure of FTBM. Arrows show hMSCs in the hydrogel layer or on the porous skeletal structure. Scale bars: 50 μ m; 500 μ m; magnifications: 98 \times ; 12.8 \times . (G) Protein expression of actin in hMSCs cultured in FTBM, as detected by immunofluorescence staining. Red arrows indicate actin expression in cells. Scale bars: 50 μ m; magnifications: 230 \times .

hMSCs within FTBM exhibited osteogenic differentiation performance equivalent to that of conventionally cultured cells. To further verify the regulatory effect of the cell-laden scaffold on osteogenic differentiation, hMSCs were isolated from FTBM, and five groups of cells were analyzed by Western blot, ALP assay, ARS staining, and RT-PCR. ALP assay showed significantly higher ALP activity in the Ber and anti138 groups, and ARS staining confirmed the

highest mineralized nodule formation rate in these two groups (Figure 4C). Western blot results confirmed that the osteogenic differentiation marker proteins ALP and RUNX2 were significantly upregulated in Ber and anti138-treated groups (Figure 4D and 4E, Figure S3). RT-PCR results were consistent with the western blot band quantification (Figure 4F); ALP and RUNX2 expression were elevated by nearly 100% and 74.29% in the Ber group, and by 75.89%

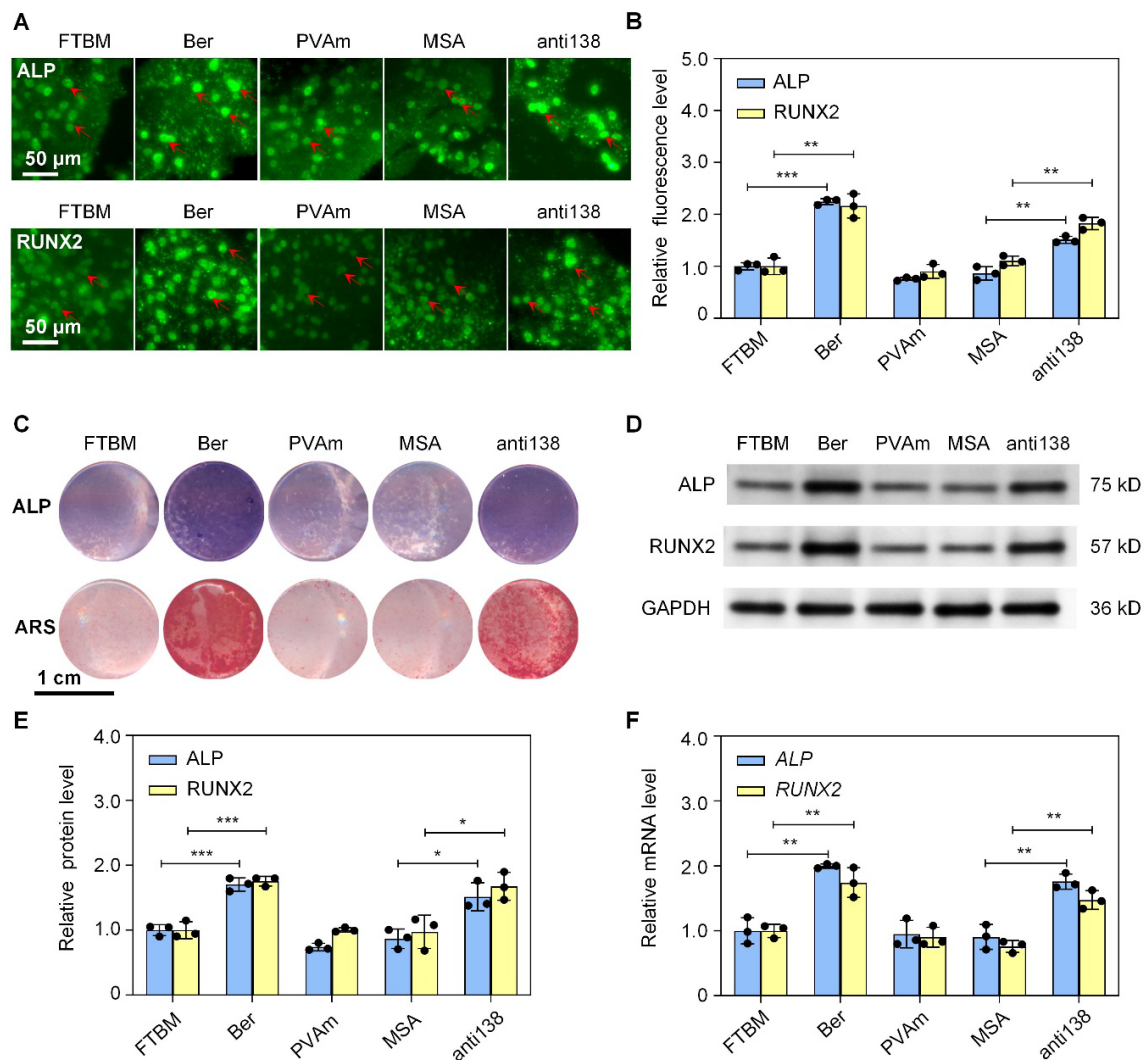


Figure 4. Fortified trabeculae-like biomimetic bone-filling material (FTBM) cell-laden scaffold regulates osteogenic differentiation *in vitro*. (A) Immunofluorescence images showing the expression of alkaline phosphatase (ALP) and runt-related transcription factor 2 (RUNX2) in human mesenchymal stem cells (hMSCs) cultured in FTBM. Red arrows indicate ALP and RUNX2 expression in cells. Scale bar: 50 μ m. (B) Fluorescence quantitative analysis, including FTBM, bergamottin (Ber), polyvinylamine (PVAm), MSA, and nCAR-anti-138 (anti138) (data represented as mean \pm standard deviation, $**p < 0.01$, $n = 3$). (C) Representative ALP and Alizarin Red staining (ARS) of hMSCs embedded in hyaluronic acid methacrylate (HAMA) hydrogel or FTBM cultured *in vitro*, treated with FTBM-loaded Ber or anti138. Scale bar: 1 cm; magnification: 1.44 \times . (D–F) Western blot images (D–E) and reverse transcription polymerase chain reaction quantification (F) showing the expression levels of ALP and RUNX2 in hMSCs cultured in FTBM. Data represented as mean \pm standard deviation; $*p < 0.05$, $**p < 0.01$, $***p < 0.001$; $n = 3$).

Notes: anti138: FTBM Embedding hMSCs and loaded with nCAR-anti-138; Ber: FTBM Embedding hMSCs and loaded with bergamottin; Blank: FTBM Embedding hMSCs without additional cargo; FTBM: Blank FTBM embedding hMSCs; MSA: FTBM Embedding hMSCs and loaded with empty recombinant tRNA; PVAm: FTBM Embedding hMSCs and loaded with polyvinylamine.

and 47.50% in the anti138 group versus blank FTBM. These demonstrate that drug-loaded FTBM supports enhanced osteogenic differentiation of embedded hMSCs.

Based on these results, *in vivo* experiments were conducted by subcutaneously implanting hMSC-encapsulated FTBM onto the calvaria surface of donor mice (Figure 5A). Mouse calvaria were harvested on day 7, and the implanted materials were collected for cell viability detection. Results showed that *in vivo* implantation did not have a cytotoxic effect on the embedded hMSCs (Figure 5B). Additionally, FTBM implantation caused no hepatorenal toxicity in mice (Figure 5C and 5D), and no significant changes in the expression levels of the inflammatory factors CD3 and CD68 in the attached bone tissue (Figure 5E). ALP and RUNX2 immunofluorescence imaging showed that Ber and anti138 groups exhibited upregulated ALP and RUNX2 expression in embedded hMSCs *in vivo* (Figure 5F and 5G). hMSCs extracted from FTBM were further analyzed using ALP assay, ARS staining, and RT-PCR, and results were consistent with the immunofluorescence results (Figure 5H and 5I). These findings demonstrated that FTBM can encapsulate cells without impairing the physiological properties of the embedded cells or the host, confirming its feasibility as a highly biocompatible bone-filling material and its potential to serve as a cell-laden scaffold.

3.4. Therapeutic effect of fortified trabeculae-like biomimetic bone-filling material on bone defects

To evaluate the therapeutic effect of FTBM on bone defects, mouse models of calvarial and tibial bone defects were established, and FTBM loaded with Ber or anti138 was implanted into the defect sites (Figure 6A and 6B). Mouse calvaria and tibiae were harvested 12 days later to assess the therapeutic efficacy. FTBM implantation caused no hepatorenal toxicity (Figure S4A–S4D) and did not affect the histomorphology of the liver, spleen, or kidney (Figure S4E), confirming the excellent *in vivo* biocompatibility of FTBM. Calcein staining and micro-computed tomography analysis confirmed that FTBM successfully filled the bone defect area and significantly enhanced bone defect repair (Figure 6C–6F).

For tibial mineral apposition rate (MAR; Figure 6G), the mean value in the Ber group was 2.3076 $\mu\text{m}/\text{d}$, an increase of 130.76% relative to the FTBM group; the anti138 group exhibited a MAR of 1.5661 $\mu\text{m}/\text{d}$, representing a 56.61% elevation compared with the FTBM group. BMD (Figure 6H) and BV/TV (Figure 6I) also presented higher values in the two drug-loaded groups. Calvarial bone defects also presented the same trend in Ber- or anti138-incorporated FTBM. Collectively, quantitative micro-computed tomography and calcein labeling data confirm that FTBM acts as a suitable bone substitute scaffold to facilitate bone

defect reconstruction. Moreover, a group of independent mice models for pharmacokinetic analysis in mice with tibial defects implanted with anti138-loaded FTBM showed that the inhibitory effect of anti138 in the tibia persisted for 28 days without significant influence on other organs (Figure S5A–S5H), indicating the *in situ* therapeutic potential of FTBM.

To further compare the therapeutic efficacy of FTBM and TBM, a mouse model with a tibial bone defect was established, and FTBM or TBM was implanted into the defect site. Four weeks later, mouse tibiae were harvested for evaluation. Micro-computed tomography and calcein staining showed that FTBM loaded with Ber or anti138 significantly enhanced bone defect repair and increased MAR, BMD, BV/TV, and BMC (Figure 7A–7F). For the FTBM series, Ber loading raised MAR by 113.24%, BMD by 91.67%, BV/TV by 93.42%, and BMC by 278.62%; anti138 treatment elevated these metrics by 74.79%, 69.06%, 74.73% and 222.94%, respectively. Notably, FTBM exhibited superior therapeutic efficacy for tibial defect repair compared with TBM, indicating greater potential for treating tibial defects.

4. Discussion

Currently, bone defect treatments mainly rely on the surgical implantation of bone-filling materials and on the body's intrinsic self-healing capacity. As bone substitutes in bone defect treatments, bone-filling materials require not only good biocompatibility but also sufficient hardness to provide mechanical support.³³ Additionally, promoting osteoblast differentiation, bone formation and repair is essential.^{34–35} In this study, our TBM² was modified by incorporating mammoth tusk dentin into its porous scaffold structures, forming an FTBM. Mammoth tusk dentin greatly enhanced the stability of porous scaffolds and effectively improved compressive strength, thereby enabling greater structural stability/maintenance at repair sites.

The FTBM consisted of a central porous scaffold and an outer hydrogel layer, the former fabricated by adding mammoth tusk dentin to the original TBM scaffold.² Mammoth tusk dentin powder mixed with biphasic calcium phosphate was then encapsulated by an organic phase composed of chitosan, collagen, and silk fibroin, which were covalently integrated into a monolithic structure via a two-step freeze-drying process. Given the high yields and reserves of mammoth ivory in the Siberian permafrost, its cost was lower than that of human dental and bone tissue, thereby helping keep FTBM costs relatively low. Furthermore, mammoth tusk dentin in FTBM was mixed with dentin, which, as in TBM, allowed integration of new bone and filling material without exerting stress shielding during bone regeneration. Incorporating mammoth

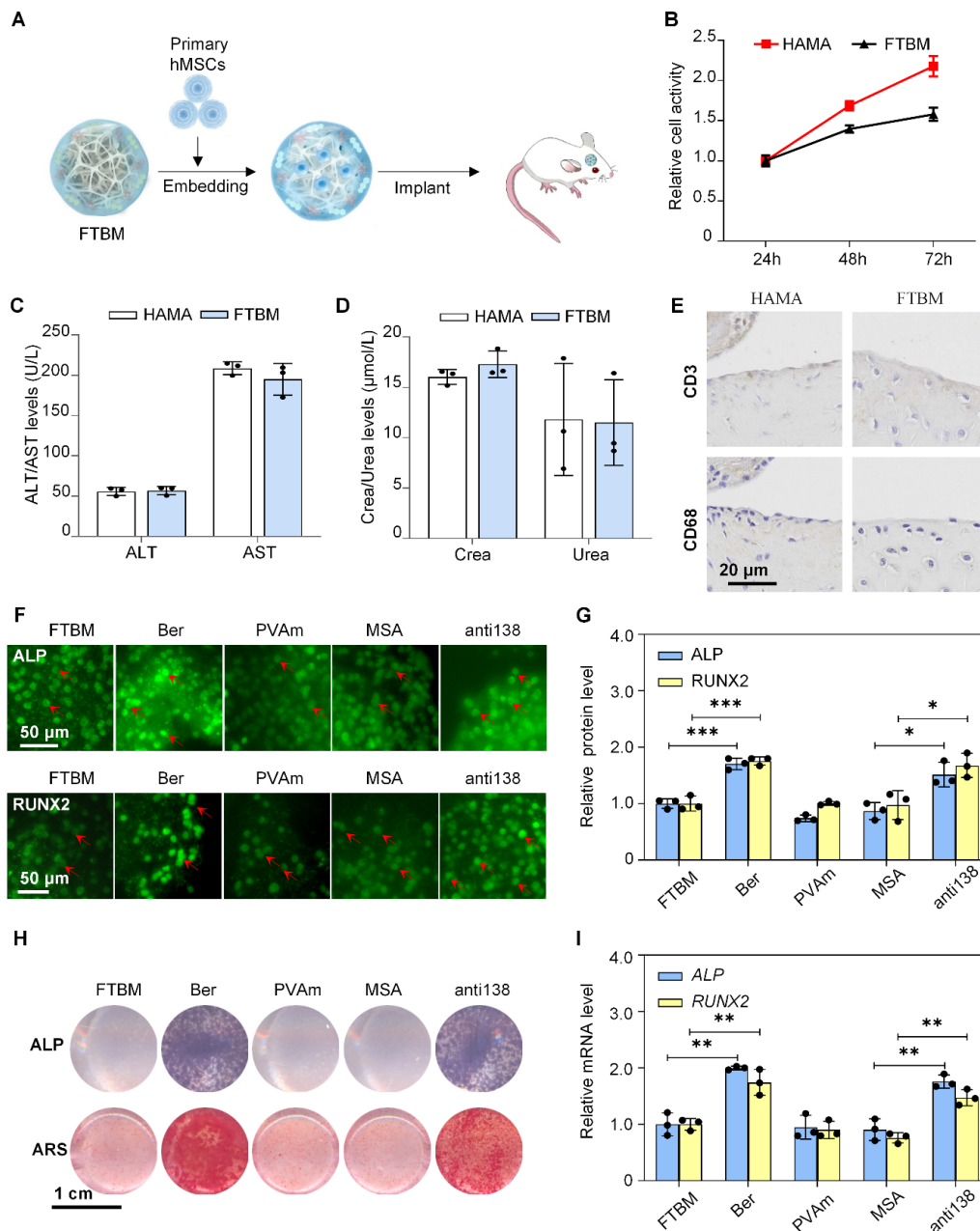


Figure 5. Fortified trabeculae-like biomimetic bone-filling material (FTBM) cell-laden scaffold regulates osteogenic differentiation *in vivo*. (A) Schematic diagram of the FTBM embedding hMSCs *in vivo*. (B) Cell viability of human mesenchymal stem cells (hMSCs) embedded in cell-laden scaffold-implanted mice, as detected by Cell Counting Kit-8. (C & D) Alanine transaminase (ALT), aspartate aminotransferase (AST), creatinine (Crea), and blood urea nitrogen (Urea) levels in blood serum of cell-laden scaffold-implanted mice (mean \pm standard deviation; $n = 3$). (E) Images of immunohistochemical staining of inflammatory factors CD3 and CD68 in calvaria of cell-laden scaffold-implanted mice. Scale bar: 20 μ m; magnification: 350 \times . (F & G) Expression of alkaline phosphatase (ALP) and runt-related transcription factor 2 (RUNX2) in cell-laden scaffold-implanted mice *in vivo* for seven days, as detected by immunofluorescence staining. Scale bar: 50 μ m; magnification: 182 \times . Red arrows indicate the ALP and RUNX2 expression in cells. Data represented as mean \pm standard deviation; $*p < 0.05$, $***p < 0.001$; $n = 3$). (H) ALP and Alizarin Red staining (ARS) of hMSCs embedded in cell-laden scaffold-implanted mice treated with FTBM loaded with bergamottin (Ber) or nCAR-anti-138 (anti138). Scale bar: 1 cm; magnification: 1.44 \times . (I) Representative reverse transcription polymerase chain reaction analysis of the expression levels of ALP and RUNX2 in hMSCs embedded in cell-laden scaffold-implanted mice. Data represented as mean \pm standard deviation; $**p < 0.01$; $n = 3$).

Notes: anti138: FTBM Embedding hMSCs and loaded with nCAR-anti-138; Ber: FTBM Embedding hMSCs and loaded with bergamottin; Blank: FTBM Embedding hMSCs without additional cargo; FTBM: Blank FTBM embedding hMSCs; MSA: FTBM Embedding hMSCs and loaded with empty recombinant tRNA; PVAm: FTBM Embedding hMSCs and loaded with polyvinylamine.

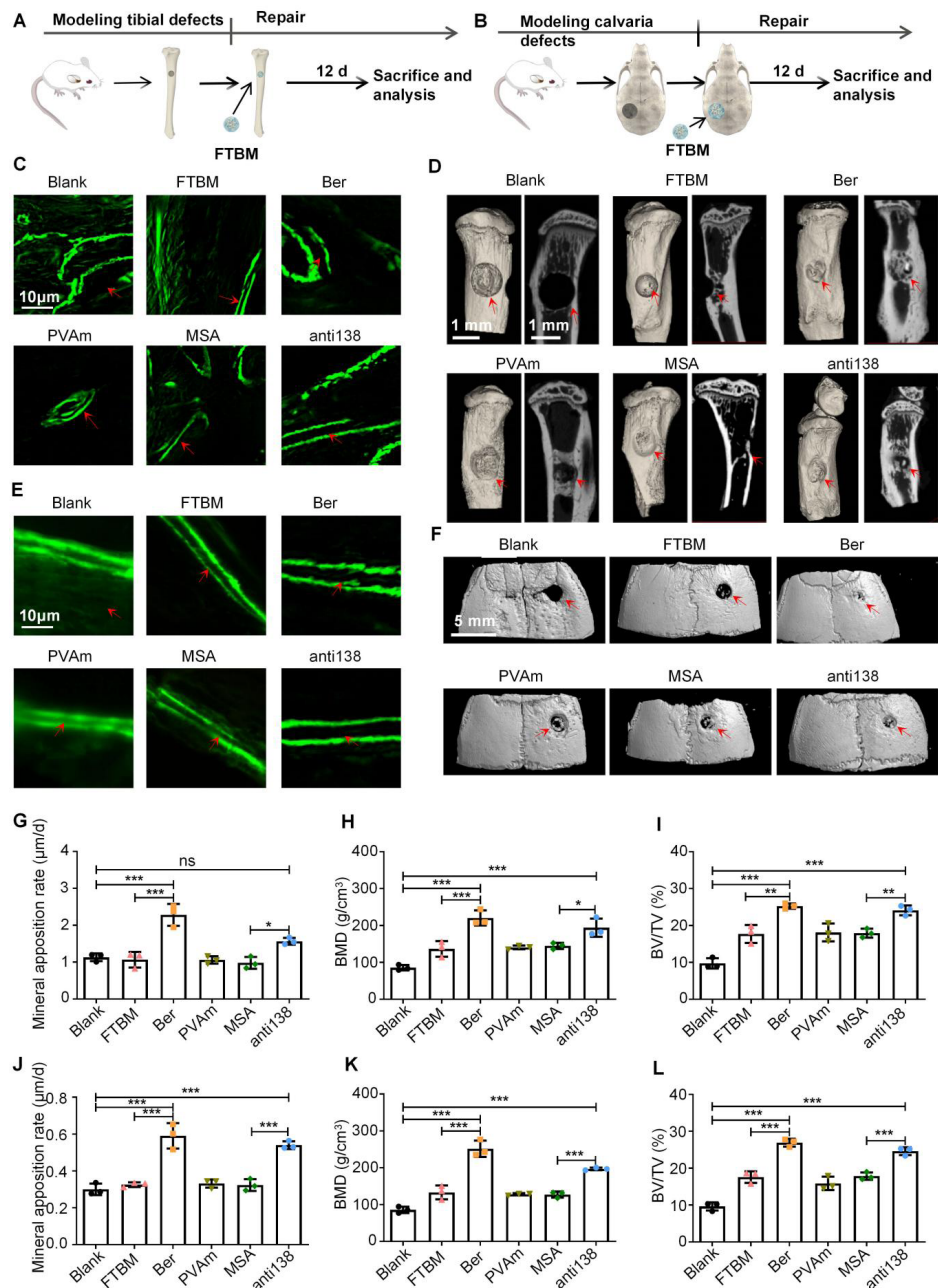


Figure 6. Effect of the fortified trabeculae-like biomimetic bone-filling material (FTBM) on *in situ* bone regeneration in tibial and calvarial defect mice. (A & B) Schematic diagram of FTBM treatment on tibial (A) and calvaria (B) defect mice. (C) Representative images showing mineral apposition rate (MAR) of the mice's tibial defect region. Scale bar: 10 μ m; magnification: 700 \times . Red arrows indicate the bone formation line distance labeled with calcein. (D) Micro-computed tomography reconstructed images of the tibial defect after 12 days. Red arrows indicate a bone defect area. Scale bar: 1 mm; magnification: 4.5 \times . (E) Representative images showing MAR of the mouse calvaria defect region. Scale bar: 10 μ m; magnification: 700 \times . Red arrows indicate the bone formation line distance labeled with calcein. (F) Micro-computed tomography reconstructed images of calvaria defect after 12 days. Red arrows indicate a bone defect area. Scale bar: 5 mm; magnification: 2 \times . (G) Quantitative analysis of the MAR in (C), data represented as mean \pm standard deviation (SD); * p < 0.05, *** p < 0.001, ns: not significant; n = 3. (H & I) Quantitative analyzes of bone mineral density (BMD) and bone volume to tissue volume (BV/TV) in (D). Data represented as mean \pm SD; * p < 0.05, ** p < 0.01, *** p < 0.001; n = 3. (J) Quantitative analysis of the MAR in (E), data represented as mean \pm SD; *** p < 0.001; n = 3. (K & L) Quantitative analyzes of BMD and BV/TV in (F). Data represented as mean \pm SD; *** p < 0.001; n = 3.

Notes: Blank: Untreated bone defects. FTBM: Bone defects implanted with blank FTBM; Ber: Bone defects implanted with FTBM and loaded with Ber; PVAm: Bone defects implanted with FTBM and loaded with polyvinylamine; MSA: Bone defects implanted with FTBM and loaded with polyvinylamine and empty recombinant tRNA; anti138: Bone defects implanted with FTBM and loaded with polyvinylamine and nCAR-anti-138.

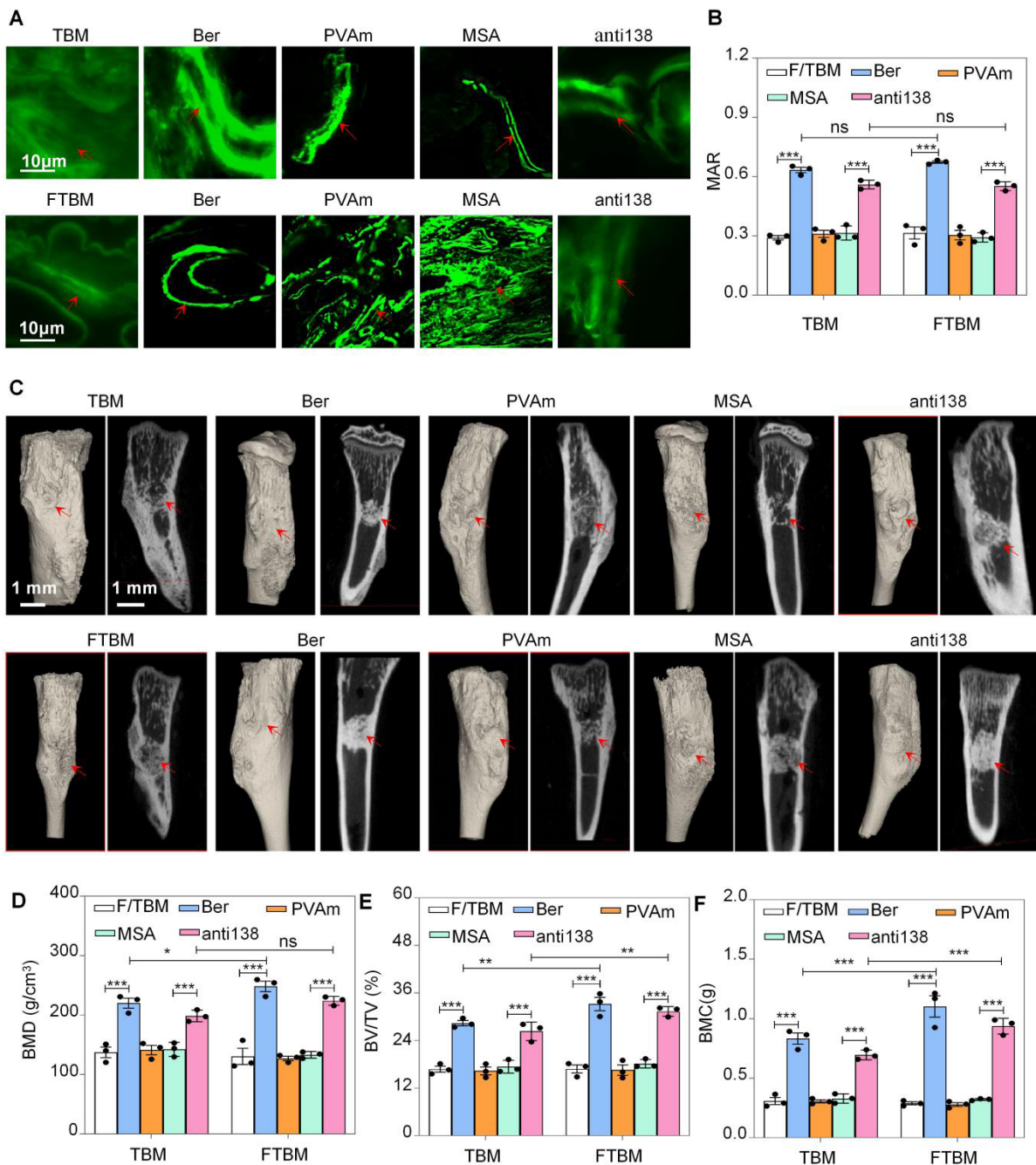


Figure 7. Comparison of the effect of the fortified trabeculae-like biomimetic bone-filling material (FTBM) and TBM on *in situ* bone regeneration in tibial defect mice. (A) Representative images showing the mineral apposition rate (MAR) of mice's tibial defect regions. Scale bar: 10 μm; magnification: 700×; and (B) quantitative analysis of the MAR. Red arrows indicate the bone formation line distance labeled with calcein. Data represented as mean ± standard deviation (SD); *** $p < 0.001$, ns: not significant; $n = 3$. (C) Micro-computed tomography reconstructed images of the tibial defect after four weeks. Scale bar: 1 mm; magnification: 4.5×. Red arrows indicate bone defect areas. (D–F) Quantitative analyzes of the (D) bone mineral density (BMD), (E) bone volume to tissue volume (BV/TV), and (F) bone mineral content (BMC) in (C). Data represented as mean ± SD; * $p < 0.05$, ** $p < 0.01$, *** $p < 0.001$, ns: not significant; $n = 3$.

Notes: Blank: Untreated bone defects. TBM: Bone defects implanted with blank TBM; FTBM: Bone defects implanted with blank FTBM; F/TBM: Bone defects implanted with blank TBM or FTBM; Ber: Bone defects implanted with FTBM and loaded with Ber; PVAm: Bone defects implanted with FTBM and loaded with polyvinylamine; MSA: Bone defects implanted with FTBM and loaded with polyvinylamine and empty recombinant tRNA; anti138: Bone defects implanted with FTBM and loaded with polyvinylamine and nCAR-anti-138.

tusk dentin powder into FTBM conferred superior mechanical properties compared to TBM, while retaining porous scaffold structures with high biocompatibility and biodegradability. Additionally, porous scaffolds were wrapped in an HAMA hydrogel that provided cushioning and drug-delivery capabilities. This hydrogel was prepared by crosslinking water-soluble HAMA and the DMSO-soluble photoinitiator Irgacure 2959. The HAMA aqueous phase carries water-soluble nucleic acid drugs, while the organic phase delivers organic-soluble drugs, thereby enabling synergistic, multi-drug delivery.³⁶

To further explore FTBM as a cell-laden scaffold, RGD peptides were incorporated into both porous scaffolds and HAMA during the FTBM design process to improve cell adhesion in the hydrogel and material. hMSCs were then attached to the material; these cells possess excellent osteogenic potential.³⁷⁻³⁸ Thus, hMSCs in FTBM, similar to TBM, attached to the cell-laden scaffold and underwent normal differentiation and migration *in vitro* and *in vivo*, indicating that FTBM was a favorable cell-laden scaffold. Due to its higher stiffness than TBM, FTBM exhibited better therapeutic effects in treating tibial bone defects and may serve as a load-bearing filler in future studies. However, unlike TBM, which is an all-natural bone-filling material, FTBM contained low mammoth tusk dentin levels. Thus, it remains unclear whether this dentin is completely resorbed by the body after bone defect repair, or whether residual dentin may exert adverse effects. Additionally, bone-related cells are highly mechanosensitive in bone tissue. When compared with TBM, FTBM had superior mechanical strength. Future research is required to construct and verify the mechanical loading model to further elucidate the underlying molecular mechanism. However, the specific effects of FTBM as a mechanical loading model, including the regulation of mechanically loading-responsive cells in bone tissue, its intervening effects on osteogenic repair, and the dynamic changes in its own mechanical properties, as well as the underlying molecular mechanisms and regulatory pathways through which it functions, remain under investigation.

5. Conclusion

In this study, FTBM, a novel composite bone-filling material with high stiffness, was fabricated by adding mammoth tusk dentin to TBM. FTBM enabled the sustained release of small-molecule and nucleic acid drugs. Within the non-load-bearing (calvarial) and tibial models tested, the reinforced construct improved osteogenic outcomes; extension to genuine load-bearing sites will require constructs with markedly higher bulk strength and appropriate large-animal models. Our study provides a promising strategy for treating bone defects and novel insights to advance bone tissue engineering research.

Acknowledgments

None.

Funding

This work was supported by the National Natural Science Foundation of China (82272436, 32371371), the Science and Technology Innovation Talent Program of Xinjiang Tianshan Talented Youth Top Talent Project, the Natural Science Foundation of Xinjiang Uygur Autonomous Region (2022D01F49), the Clinical Research Program of Affiliated Hospital of North Sichuan Medical College (2021LC008), the North Sichuan Medical College Innovation Team (Natural Science: CBYTD-2025A04), the Doctoral Research Startup Fund Project of the Affiliated Hospital of North Sichuan Medical College (BS10001, CBY19-QD01), and the Innovation and Entrepreneurship project of North Sichuan Medical College (XJ202510634159, XJ202510634155, XJ202510634157, XJ202510634153, XJ202510634151).

Conflict of interest

The authors declare no conflict of interest.

Author contributions

Conceptualization: Chong Yin, Xingyu Wang, Yingying Luo, Ye Tian, Bing Yang, Wei Chen, Bing Guo, Xundong Deng, Guangrong Wang

Formal analysis: Chong Yin, Xingyu Wang, Jing Zhang, Linfeng Liu, Hongqi Han, Guilin Luo, Zhuo Guo, Yingying Luo, Jingxiang Li

Investigation: Chong Yin, Xingyu Wang, Jing Zhang, Linfeng Liu, Hongqi Han, Guilin Luo, Zhuo Guo, Yingying Luo, Conghui Jiang, Rui Pang, Jingxiang Li

Methodology: Chong Yin, Guangrong Wang, Ye Tian, Bing Yang, Wei Chen, Bing Guo, Xundong Deng

Writing—original draft: Chong Yin, Xingyu Wang, Y.Y., Jing Zhang

Writing—review & editing: Chong Yin, Xingyu Wang, Jing Zhang, Linfeng Liu, Hongqi Han, Guilin Luo, Zhuo Guo, Yingying Luo, Conghui Jiang, Rui Pang, Jingxiang Li, Xundong Deng, Guangrong Wang

All authors read and approved the final manuscript.

Ethics approval and consent to participate

Animal care/procedures were sanctioned by the North Sichuan Medical College Ethics Committee (No. 2023078). At all times, we minimized the number of mice and their suffering during animal studies.

Consent for publication

Not applicable.

Availability of data

The datasets used and/or analyzed during the current study

are available from the corresponding author (Guangrong Wang, 13699669835@163.com) on reasonable request.

References

1. Sparks DS, Saifzadeh S, Savi FM, *et al.* A preclinical large-animal model for the assessment of critical-size load-bearing bone defect reconstruction. *Nat Protoc.* 2020;15(3):877-924. doi: 10.1038/s41596-019-0271-2
2. Meng F, Yu Y, Yu J, *et al.* A trabeculae-like biomimetic bone-filling material as a potential cell-laden scaffold for bone defect treatment. *Cell-Laden Scaffold Res.* 2025;1(2):025040003. doi: 10.36922/OR025040003
3. De La Vega RE, van Griensven M, Zhang W, *et al.* Efficient healing of large osseous segmental defects using optimized chemically modified messenger RNA encoding BMP-2. *Sci Adv.* 2022;8(7):eabl6242. doi: 10.1126/sciadv.abl6242
4. Wang Z, Lv ZH, Cai XJ, *et al.* Sculpting the Future of Bone: The Evolution of Absorbable Materials in Orthopedics. *Adv Mater.* 2026;38(9):e2510848. doi: 10.1002/adma.202510848
5. Yin C, Deng M, Yu J, *et al.* An Andrias davidianus derived composite hydrogel with enhanced antibacterial and bone repair properties for osteomyelitis treatment. *Sci Rep.* 2024;14(1):24626. doi: 10.1038/s41598-024-75997-8
6. Salamanca E, Hsu C, Huang H, *et al.* Bone regeneration using a porcine bone substitute collagen composite *in vitro* and *in vivo*. *Sci Rep.* 2018;8(1):984. doi: 10.1038/s41598-018-19629-y
7. Zhang J, Zhang W, Yue W, Qin W, Zhao Y, Xu G. Research Progress of Bone Grafting: A Comprehensive Review. *Int J Nanomed.* 2025;20:4729-4757. doi: 10.2147/IJN.S510524
8. Gui X, Peng W, Xu X, *et al.* Synthesis and application of nanometer hydroxyapatite in biomedicine. *Nanotechnol Rev.* 2022;11(1):2154-2168. doi: 10.1515/ntrev-2022-0127
9. Dec P, Modrzejewski A, Pawlik A. Existing and novel biomaterials for bone tissue engineering. *Int J Mol Sci.* 2023;24(1):529. doi: 10.3390/ijms24010529
10. Duan H, Cao C, Wang X, *et al.* Magnesium-alloy rods reinforced bioglass bone cement composite scaffolds with cortical bone-matching mechanical properties for load-bearing bone *in vivo* regeneration. *Sci Rep.* 2020;10(1):18193. doi: 10.1038/s41598-020-75328-7
11. Xu Y, Sheng L, Zhu M, *et al.* From niche to organoid: Engineering bone tissues through microenvironmental insights. *J Tissue Eng.* 2025;16:1-25. doi: 10.1177/20417314251358567
12. Lin S, Narayanan K, Vashishth D. Bone Organoids: A Novel Tool for Modeling and Managing Skeletal Disorders in Diabetes. *Adv Sci.* 2026;38:e2518788. doi: 10.1002/advs.202518788
13. Wei HP, Cui JJ, Lin KL, *et al.* Recent advances in smart stimuli-responsive biomaterials for bone therapeutics and regeneration[J]. *Bone Res.* 2022;10(1):58. doi: 10.1038/s41413-021-00180-y
14. Taherian MH, Le TA, Le AVT, *et al.* Controlled microstructural evolution of hydroxyapatite-Bioglass® nanocomposites via two-step sintering. *J Mech Behav Biomed Mater.* 2026;175:107329. doi: 10.1016/j.jmbbm.2025.107329
15. Arantes Fernandes Vieira L, Marinho JPN, de Sousa RG, *et al.* Development of a composite based on hydroxyapatite, carboxymethyl cellulose, and boron nitride nanotubes as a potential material for bone graft. *ACS Appl Eng Mater.* 2025;3(11):3964-3975. doi: 10.1021/acsaenm.5c00679
16. Qi L, Zhao T, Yan J, *et al.* Advances in magnesium-containing bioceramics for bone repair. *Biomater Transl.* 2024;5(1):3-20. doi: 10.12336/biomatertransl.2024.01.002
17. Liang J, Lu X, Zheng X, *et al.* Modification of titanium orthopedic implants with bioactive glass: a systematic review of *in vivo* and *in vitro* studies. *Front Bioeng Biotechnol.* 2023;11:1269223. doi: 10.3389/fbioe.2023.1269223
18. Mani N, Sola A, Trinchì A, Fox K. Is there a future for additive manufactured titanium bioglass composites in biomedical application? A perspective. *Biointerphases.* 2020;15(6):068501. doi: 10.1116/6.0000557
19. Fu Q, Saiz E, Rahaman MN, *et al.* Bioactive glass scaffolds for bone tissue engineering: state of the art and future perspectives. *Mater Sci Eng C Mater Biol Appl.* 2011;31(7):1245-1256. doi: 10.1016/j.msec.2011.04.022
20. Oliver-Urrutia C, Kashimbetova A, Slámečka K, *et al.* Porous titanium/hydroxyapatite interpenetrating phase composites with optimal mechanical and biological properties for personalized bone repair. *Biomater Adv.* 2025;166:214079. doi: 10.1016/j.bioadv.2024.214079
21. Shen M, Lu Z, Xu Y, *et al.* Vivianite and its oxidation products in mammoth ivory and their implications to the burial process. *ACS Omega.* 2021;6(34):22284-22291. doi: 10.1021/acsomega.1c02964
22. van der Valk T, Pečnerová P, Díez-Del-Molino D, *et al.*

- Million-year-old DNA sheds light on the genomic history of mammoths. *Nature*. 2021;591(7849):265-269.
doi: 10.1038/s41586-021-03224-9
23. Zhao L, Li X, Zhao J, *et al.* A novel smart injectable hydrogel prepared by microbial transglutaminase and human-like collagen: its characterization and biocompatibility. *Mater Sci Eng C Mater Biol Appl*. 2016;68(1):317-326.
doi: 10.1016/j.msec.2016.05.108
 24. Tian Y, Zhao Y, Yin C, *et al.* Polyvinylamine with moderate binding affinity as a highly effective vehicle for RNA delivery. *J Control Release*. 2022;345:20-37.
doi: 10.1016/j.jconrel.2022.03.003
 25. Hu L, Su P, Li R, *et al.* Knockdown of microtubule actin crosslinking factor 1 inhibits cell proliferation in MC3T3-E1 osteoblastic cells. *BMB Rep*. 2015;48(10):583-588.
doi: 10.5483/bmbrep.2015.48.10.098
 26. Liu G, Wang L, He Y, *et al.* Polydopamine nanosheets doped injectable hydrogel with nitric oxide release and photothermal effects for bacterial ablation and wound healing. *Adv Healthc Mater*. 2021;10(23):e2101476.
doi: 10.1002/adhm.202101476
 27. Hu L, Yin C, Chen D, *et al.* MACF1 promotes osteoblast differentiation by sequestering repressors in cytoplasm. *Cell Death Differ*. 2021;28(7):2160-2178.
doi: 10.1038/s41418-021-00744-9
 28. Li K, Chen Y, Lin Y, *et al.* PD-1/PD-L1 blockade is a potent adjuvant in treatment of Staphylococcus aureus osteomyelitis in mice. *Mol Ther*. 2023;31(1):174-192.
doi: 10.1016/j.ymthe.2022.09.006
 29. Ushiku C, Adams DJ, Jiang X, *et al.* Long bone fracture repair in mice harboring GFP reporters for cells within the osteoblastic lineage. *J Orthop Res*. 2010;28(10):1338-1347.
doi: 10.1002/jor.21105
 30. Yin C, Tian Y, Li D, *et al.* Long noncoding RNA Lnc-DIF inhibits bone formation by sequestering miR-489-3p. *iScience*. 2022;25(3):103949.
doi: 10.1016/j.isci.2022.103949
 31. Wang X, Tian Y, Liang X, *et al.* Bergamottin promotes osteoblast differentiation and bone formation via activating the Wnt/ β -catenin signaling pathway. *Food Funct*. 2022;13(5):2913-2924.
doi: 10.1039/d1fo02755g
 32. Chen Z, Zhao F, Liang C, *et al.* Silencing of miR-138-5p sensitizes bone anabolic action to mechanical stimuli. *Theranostics*. 2020;10(26):12263-12278.
doi: 10.7150/thno.53009
 33. Kuczkowski M, Kotwica K. Biocompatible thermoplastics in additive manufacturing of bone defect fillers: state-of-the-art and future prospects. *Materials*. 2025;18(16):3723.
doi: 10.3390/ma18163723
 34. Naini A, Rachmawati D, Cholid Z, *et al.* Enhanced osteogenic marker expression in alveolar bone via hydroxyapatite gypsum puger-cassava starch scaffold: an *in vivo* study. *J Indian Prosthodont Soc*. 2025;25(3):258-265.
doi: 10.4103/jips.jips_97_25
 35. Fernandez de Grado G, Keller L, Idoux-Gillet Y, *et al.* Bone substitutes: a review of their characteristics, clinical use, and perspectives for large bone defects management. *J Tissue Eng*. 2018;9:2041731418776819.
doi: 10.1177/2041731418776819
 36. Pérez-Lloret M, Erxleben A. Improved and highly reproducible synthesis of methacrylated hyaluronic acid with tailored degrees of substitution. *ACS Omega*. 2024;9(24):25914-25921.
doi: 10.1021/acsomega.4c00372
 37. Pittenger MF, Mackay AM, Beck SC, *et al.* Multilineage potential of adult human mesenchymal stem cells. *Science*. 1999;284(5411):143-147.
doi: 10.1126/science.284.5411.143
 38. Lee M, Jeong SY, Ha J, *et al.* Low immunogenicity of allogeneic human umbilical cord blood-derived mesenchymal stem cells *in vitro* and *in vivo*. *Biochem Biophys Res Commun*. 2014;446(4):983-989.
doi: 10.1016/j.bbrc.2014.03.0510